water

MDPI

Article

A Novel WTG Method for Predicting Ship Trajectories in the Fujian Inshore Area Based on AIS Data

Xurui Li [1,†], Dibo Dong [1,†], Qiaoying Guo [1,*], Chao Lin [1], Zhuanghong Wang [1] and Yiting Ding [2,*]

[1] Institute of Smart Marine and Engineering, Fujian University of Technology, Fuzhou 350118, China
[2] Finance and Economics College, Jimei University, Xiamen 361021, China
* Correspondence: gqy@fjut.edu.cn (Q.G.); dingyt@jmu.edu.cn (Y.D.)
† These authors contributed equally to this work.

Abstract: The increasing congestion in major global maritime routes poses significant threats to international maritime safety, exacerbated by the proliferation of large, high-speed vessels. To improve the detection of abnormal ship behavior, this research employed automatic identification system (AIS) data for ship trajectory forecasting. Traditional methods primarily focus on spatial and temporal correlations but often lack accuracy and reliability. In this study, ship path predictions were enhanced using the WTG model, which combines wavelet transform, temporal convolutional networks (TCN), and gated recurrent units (GRU). Initially, wavelet decomposition was applied to deconstruct the input trajectory time series. The TCN and GRU modules then extracted features from both the time series and the decomposed data. The predicted elements were reassembled using a multi-head attention mechanism and a pooling layer to produce the final predictions. Comparative experiments demonstrated that the WTG model surpasses other models in the accuracy of ship trajectory prediction. The model proposed in this study proves to be reliable for forecasting ship paths, which is crucial for marine traffic management and ensuring safe navigation.

Keywords: trajectory prediction; AIS data; wavelet transform; TCN-GRU method

check for updates

Citation: Li, X.; Dong, D.; Guo, Q.; Lin, C.; Wang, Z.; Ding, Y. A Novel WTG Method for Predicting Ship Trajectories in the Fujian Inshore Area Based on AIS Data. *Water* **2024**, *16*, 3036. https://doi.org/10.3390/w16213036

Academic Editor: Serafeim E. Poulos

Received: 7 August 2024
Revised: 9 October 2024
Accepted: 16 October 2024
Published: 23 October 2024

Copyright: © 2024 by the authors. Licensee MDPI, Basel, Switzerland. This article is an open access article distributed under the terms and conditions of the Creative Commons Attribution (CC BY) license (https://creativecommons.org/licenses/by/4.0/).

1. Introduction

Recently, the shipping industry has experienced significant growth, resulting in a substantial increase in the number of ships in certain bodies of water. This surge in traffic has resulted in issues such as crowded waterways and ship collisions, leading to substantial economic losses and posing a significant risk to personnel safety. China's coastal waters are recognized as among the most complex maritime areas in the world. Its enormous navigation density, and in particular, its large number of coastal fishing vessels, poses significant risks and challenges to ship navigation safety. Consequently, there is an increasing demand for efficient, safe, and intelligent shipping. To address this, an automatic identification system (AIS) [1] was designed to capture, transmit, and receive data related to ship navigation. More specifically, a ship located in a specific maritime region transmits the pertinent data to nearby AIS receivers. Nearby ships equipped with shipborne AIS can receive this data, which can be used to assist ship operators in making informed decisions. Furthermore, the AIS offers a substantial amount of spatial and temporal information. Through the use of this AIS data and by conducting a thorough analysis of their current and historical trajectory information, it is feasible to forecast various aspects of ship navigation, including future ship trajectories. This valuable insight serves as a reliable reference for monitoring ship traffic [2,3].

The primary objective of trajectory prediction is to enhance maritime safety by enabling ships to navigate at sea with a reduced collision risk. To date, numerous studies have been conducted using land vehicles, pedestrians, and robots that hold significant reference values [4–7]. The course of a ship is intricately linked to its navigational

characteristics, and the accuracy of extracting these features increases proportionally with the amount of available historical data. However, conventional trajectory prediction algorithms are unable to completely acquire historical ship navigation characteristics from extensive AIS data; the advent of deep learning models has effectively addressed this issue. Indeed, researchers, both domestically and internationally, have recognized the ability to forecast future paths using deep neural networks and have obtained favorable outcomes. Recently, researchers have focused on developing hybrid models to enhance the prediction accuracy [8,9]. More specifically, a hybrid model was created by combining various models and leveraging the strengths of the different modules to achieve an improved prediction accuracy.

Traditional methods for trajectory prediction primarily rely on Kalman filters, Markov chain models, and similar techniques. For example, Jiang et al. [10] enhanced the Kalman filtering algorithm to address the issue of incomplete track data and predict the positions of ships. However, their model exhibited the limited utilization of historical track information, resulting in relatively low prediction accuracy. In another study, Guo et al. [11] utilized a conventional algorithm to partition a specified sea region into grids. They determined the state of each grid by considering the position, speed, and direction of ships as crucial factors. In addition, they constructed a state transition matrix using a K-order Markov chain to make predictions. Nevertheless, these methods are only suitable for predicting the trajectory of a solitary vessel in undisturbed sea regions, and do not consider the interplay between multiple vessels in intricate and congested waters.

An increasing number of studies have demonstrated that neural networks exhibit superior performances. For example, Zhou [12] constructed a prognostic framework for ship trajectories using back-propagation (BP) neural networks. However, an inadequate quantity of historical data were used for these predictions. In addition, Hu et al. [13] performed data preprocessing using a Gauss–Kruger projection and an enhanced linear interpolation method. They subsequently utilized gated recurrent unit (GRU) models to predict the trajectories; however, they provided minimal enhancements to previous models. As an alternative approach, Quan et al. [14] utilized AIS data and a long short-term memory (LSTM) model to predict future trajectories. They employed the longitude, latitude, speed, heading, and time interval as input variables, allowing the model to predict trajectories at any time interval instead of being limited to fixed intervals. However, it should be noted that this method is simply an application of LSTM, and does not improve upon the existing approaches. However, this significantly reduced the computational efficiency of the model. Later, Zhao et al. [15] innovatively integrated a recurrent neural network (RNN) with a bidirectional long short-term memory (Bi-LSTM) network. However, the training of this two-way network required additional time.

Overall, traditional prediction methods have inherent limitations, such as the requirement to establish a ship's equation of motion, and the necessity for the trajectory to conform to a specific distribution. However, traditional methods for predicting ship movement only provide accurate results for short periods of time, owing to the intricate nature of the process. In contrast, recurrent neural networks and their variations have been validated in numerous trajectory–prediction scenarios. However, this approach has several limitations. Given the time-series nature of the ship trajectory prediction task, the trajectory attributes also incorporate frequency information. The time series of the longitude, latitude, course over ground (COG), and speed over ground (SOG) respond to changes in the ship motion, as determined by the navigational intent and local details. However, the current method primarily emphasizes modeling in the time domain, and analysis of the time-frequency remains an unexplored area in ship trajectory prediction research, lacking the intricate examination of frequency details. Thus, drawing inspiration from successful applications in other time-series forecasting tasks [16], it is believed that time-frequency analysis has great potential for capturing the underlying patterns of ship trajectories to achieve a more nuanced ship–trajectory prediction.

To enhance the training stability and to optimize the effectiveness and precision of the model predictions, the temporal convolutional network (TCN) model can be implemented. TCN is a recently developed network model that demonstrates a superior performance in time-series problems [17–19]. Indeed, several studies have demonstrated that TCN has a higher prediction accuracy than common network models in specific time-series scenarios, particularly in the case of ship trajectory sequences, which fall under the time-series category. This provides a number of benefits. For example, TCN has the ability to perform parallel data processing, and the TCN gradient exhibits greater stability. In addition, the receptive field size of TCN can be easily adjusted to suit different tasks, and the TCN network does not require a significant amount of memory.

Thus, in this study, we present a framework for ship trajectory prediction that is expected to offer a number of contributions. More specifically, we present a wavelet-based time-frequency framework to forecast ship trajectories in an innovative manner. Our methodology incorporates time-frequency analysis to capture the dynamic features of trajectories, which will be expected to improve the accuracy of ship trajectory predictions compared to other studies. In addition, the described system integrates TCN and GRU modules to analyze data features extracted post-wavelet treatment. Enhancing the extraction of concealed information and temporal correlations from diverse frequency data should improve the learning skills for ship navigation patterns in different maritime regions, therefore enhancing the predictive performance. Furthermore, we examine various aspects of the AIS data that the impact of ship navigation trajectory predictions to improve model training efficiency. A fixed-length sliding window approach is used to track the real changes and fluctuation patterns in the characteristics.

2. Materials and Methods

Initially, the AIS data were processed before inputting the refined data into the prediction model. The model was compared to several machine learning and deep learning methods using an experimental design to evaluate its prediction performance. This assessment used two historical ship trajectory datasets with different traffic patterns. The research findings were showcased through a comparative analysis to confirm the efficacy and resilience of the suggested approach. Anomalous data were eliminated from the initial AIS dataset to improve the performance of the predictive model, as illustrated in Figure 1. Attribute values with a lower correlation in the ship trajectory data were identified and maintained using a correlation analysis. Subsequently, data differentiation and normalization were conducted to guarantee data continuity. A hybrid model was employed that incorporates a wavelet transform (WT) to analyze ship navigation trajectories, considering both local details and overall trend motion features, after analyzing the AIS data. This model utilizes a TCN and a GRU to improve the processing of the sequence data, leading to increased accuracy and performance in predicting ship trajectories.

2.1. Datasets

The China Ports Network (https://www.chinaports.com, accessed on 26 March 2024) provides a significant volume of AIS data publicly, which is advantageous for studies in numerous relevant sectors [17,20]. This raw AIS data contains a significant amount of information with varying degrees of importance for predicting ship trajectories. The data consist of static and dynamic ship data, along with navigation data, including the ship's maritime mobile service identity (MMSI) unique identification code, call sign, latitude, longitude, SOG, COG, and other specific information, as detailed in Table 1.

The file contained AIS data recorded for ships between 16 March 2024 and 26 March 2024. The region of interest consisted of a rectangular area defined by the coordinates (119.6°, 24.6°) and (121.7°, 27.1°). The original dataset comprised 13,679 trajectory data points. Of these, 12,086 trajectories were employed for model training and hyperparameter tuning, while the remaining 1593 data points were designated as the test set.

Table 1. AIS Data Composition.

Static Data	Dynamic Data	Navigation Data
MMSI	Longitude	Draught
IMO Number	Latitude	Destination Port
Ship Type	SOG	Estimated Time of Arrival
Ship Length and Height	COG	
Call Sign and Ship Number	Status	

Prior to utilizing the AIS data for ship trajectory prediction, it is crucial to preprocess the data to ensure reliability and usability. Signal instability or channel congestion can lead to anomalies, such as duplicate and inaccurate AIS data. Anomaly detection strategies are utilized to eliminate abnormalities and prevent any negative impact on the model performance during tests. The data-cleaning procedure consisted of five preprocessing phases, namely anomaly identification, rapid information extraction, data interpolation, equal-interval processing, and data normalization [21].

This study employed cubic spline interpolation to preprocess the raw data, ensuring a time interval of one minute between the consecutive data points. To determine the influence of different vessel AIS data on the model output, after removing outliers, a correlation analysis was conducted on various vessel attributes to enhance computational efficiency and reduce workload. As shown in Figure 1, attributes such as draft, vessel height, and vessel width exhibited strong correlations, with correlation coefficients exceeding 0.85. In contrast, attributes like longitude, latitude, speed over ground (SOG), and course over ground (COG) showed weaker correlations. Therefore, these four variables were selected as the feature sequence for the trajectory prediction model.

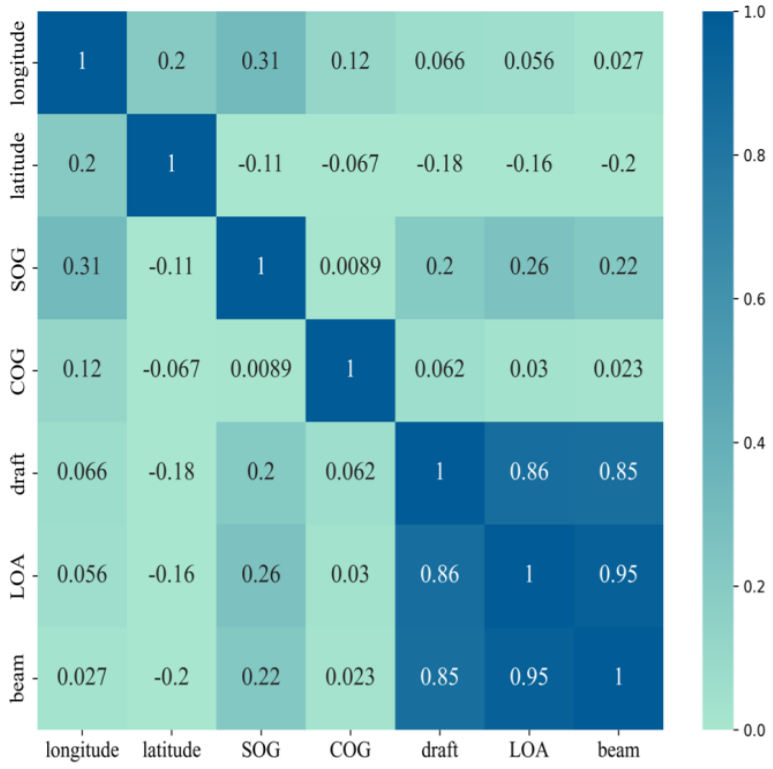


Figure 1. Correlation analysis of the different parameters.

The cubic spline interpolation method was used to interpolate the longitude and latitude at equal time intervals, and its reliable performance was validated [22,23]. To ensure that the time series data input into the model possessed equal time intervals, the

spline interpolation method was used for equal interval processing of the AIS data, where $T(t)$ in each sub-time interval $[t_i, t_{i+1}](i = 0, 1, \cdots, n-1)$, as shown in Equation (1):

$$T(t) = a_i t_i^3 + b_i t_1^2 + c_i t_1 + d_i (i = 0, 1, \cdots, n-1) \quad (1)$$

After interpolation, the time interval between the trajectories in the dataset was 1 min. Finally, the min–max normalization method was used to standardize the four data points of the longitude, latitude, SOG, and COG to unify the scale and range of the data. The definition of the normalized value x_{std} is given in Equation (2):

$$x_{std} = \frac{x_{raw} - x_{min}}{x_{max} - x_{min}} \quad (2)$$

where x_{min} is the minimum value in the data, x_{max} is the maximum value in the data, and x_{raw} is a pre-normalized value.

2.2. Problem Definition

Definition 1: Ship Trajectory. *The ship trajectory Traj is represented as a sequence of points with timestamps, i.e.,*$Traj = \{Po_1, \cdots, Po_i, \cdots, Po_N\}$. *Let* $Po_i = \{lat_i, lon_i, sog_i, cog_i\}$, $(i = 1, 2, \cdots, N)$ *where* Po_i, lat_i, lon_i, sog_i, cog_i *represent the latitude, longitude, SOG, and COG at the ith timestamp, respectively.*

Definition 2: Ship Trajectory Dataset. *Let* $TD = \{Traj_1, \cdots, Traj_j, \cdots, Traj_n\}$ *where* $j = 1, 2, \cdots, n$ *represents the ship trajectory dataset. The jth trajectory in the dataset is represented by* $Traj_j = \{Po_{j1}, \cdots, Po_{ji}, \cdots, Po_{jN}\}$.

2.3. Model Structure

To improve the accuracy of the ship trajectory prediction, a hybrid ship trajectory prediction framework was proposed, namely the WTG model. Figure 2 shows a flowchart of the WTG model, which consists of five layers, namely the input, WT, TCN, GRU, and output. The ship's historical trajectory $Po = \{lat, lon, sog, cog\}$ extracted from the AIS data were used as the input, and the future trajectory was used as the output. The WT layer used different window functions to decompose the input time-series signal into low- and high-frequency signals. The TCN layer employed causal convolutions, dilated convolutions, and residual blocks to avoid gradient vanishing or explosion problems while effectively extracting multivariate time-series information. The GRU layer was responsible for analyzing and predicting the temporal features of the decomposed and extracted trajectory data. The temporal convolutional network (TCN) is capable of extracting multi-scale features from the input sequence through its multiple convolutional layers, making it particularly adept at capturing local patterns and short-term variations. Building upon the features extracted by the TCN, the gated recurrent unit (GRU) further models the temporal dependencies within the sequence, effectively capturing more complex dynamic patterns. This layered architecture enables the model to simultaneously process both local and global temporal features, thereby enhancing its ability to adapt to the complexities inherent in AIS data [17,24,25]. In this model, the WT layer extracted time-series information at different frequencies and the TCN layer extracted multivariate interaction information. The information extracted by the two layers was then integrated and input into the GRU layer to generate potential feature trajectories. Finally, the multistep outputs of the GRU layer were fused through a multi-head attention layer and a pooling layer to output the predicted trajectory.

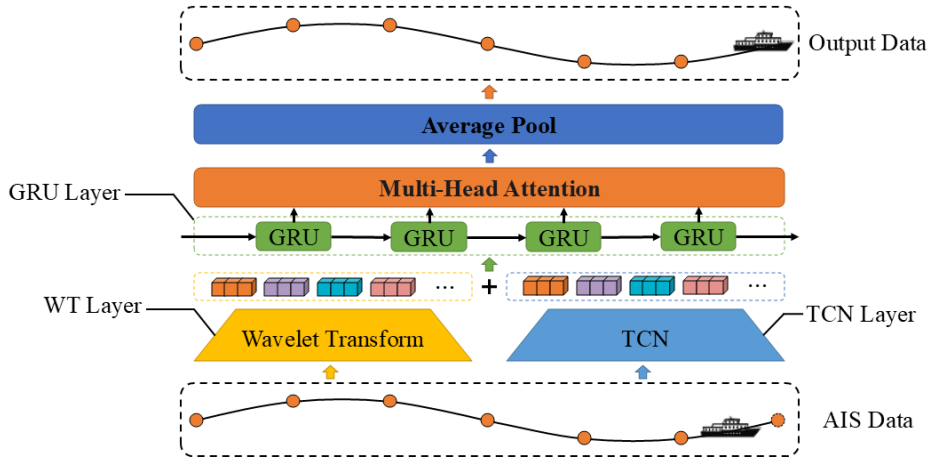


Figure 2. Flowchart of the WTG method.

2.3.1. Wavelet Transform

Wavelet transform (WT) is an essential method for time-frequency analysis, offering significant advantages over other signal processing techniques. Unlike the Short-Time Fourier Transform (STFT) [26], which employs a fixed window size, WT utilizes wavelet bases of finite lengths, allowing for better adaptability to varying signal features. This flexibility is particularly beneficial for analyzing non-stationary signals, such as ship trajectory data, where signal characteristics can change over time. Additionally, WT provides superior localization in both time and frequency domains compared to methods like Empirical Mode Decomposition (EMD) [27] and Principal Component Analysis (PCA) [28], enabling more accurate feature extraction and the capture of intricate patterns in ship movements. These advantages make WT a more suitable choice for enhancing the accuracy and reliability of ship trajectory prediction in complex marine environments. The mathematical expression is as follows:

$$\omega(a,b) = \frac{1}{\sqrt{a}} \int_{-\infty}^{+\infty} f(t) \cdot \psi\left(\frac{t-b}{a}\right) dt \tag{3}$$

where $\psi(x)$ is the wavelet basis function, a is the scaling parameter for the basis function, and b is the translation parameter that reflects the movement of the wavelet basis function along the time axis.

Previous studies have shown that the quality of the input data is crucial for determining the accuracy of the trajectory prediction. Therefore, the quality requirements for the trajectory data are particularly stringent. The discrete wavelet transform (DWT) can refine signals into subsignals of different scales. Compared to Fourier transform, it can capture and express the information contained in the data more effectively. By processing the trajectory data with DWT, noise can be effectively reduced, rendering the input trajectory characteristics clearer and more distinct.

The DWT used in this study employs the Daubechies wavelet as the basis function. Due to its good regularity properties, the Daubechies wavelet introduces smoothing errors that are difficult to detect when used on a sparse basis, thereby rendering the signal reconstruction process smoother. The basis function $\psi(x)$ is given by

$$\psi(x) = \sum_{k=0}^{M-1} b_k \phi(2x-k) \tag{4}$$

where $\phi(x)$ is expressed as

$$\phi(x) = \sum_{k}^{M} a_k \phi(2x-k) \tag{5}$$

2.3.2. Temporal Convolutional Network

In 2018, Bai et al. introduced the TCN [17], an algorithm specifically designed for time-series data analysis. TCN features three key innovations: causal convolution, dilated convolution, and residual modules, all aimed at effectively capturing long-term dependencies in time-series information for accurate future predictions.

Causal convolution is the fundamental architecture of TCN. As shown in Figure 3, assuming the input sequence is $X = (x_0, x_1, \cdots, x_t, \cdots, x_T)$, the causal convolution stack precisely ensures that the output y_t at any given time t depends only on the current input x_t and its past inputs $(x_0, x_1, \cdots, x_{t-1})$, effectively isolating it from any future inputs $(x_{t+1}, x_{t+2}, \cdots, x_T)$. Two key reasons exist for adopting this architectural design. Firstly, it ensures that the network output depends solely on previous input data, thereby eliminating the risk of future data "leaking" into past analysis. Secondly, this restriction underscores a key trade-off in TCN design, ensuring causality and temporal accuracy. Although this design enforces temporal integrity, it inherently limits the network's receptive field, restricting it to use only limited historical data for prediction.

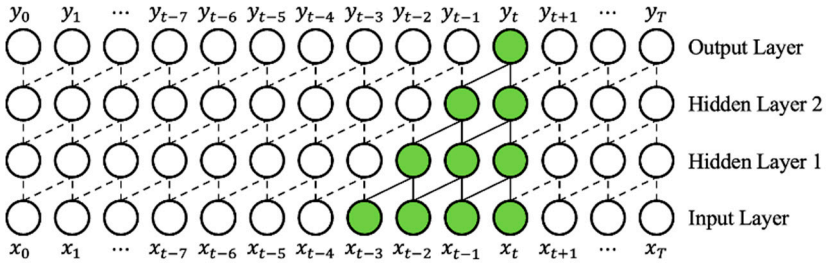


Figure 3. Causal convolution structure.

TCN effectively addresses the issue of limited receptive fields by introducing dilated convolution techniques within the framework of causal convolution. As shown in Figure 4, for a given one-dimensional time series input $X = (x_0, x_1, \cdots, x_t, \cdots, x_T)$ and a defined filter $f : \{0, 1, 2, \cdots, n-1\}$,the dilated convolution operation of the sequence element $Traj$ can be expressed as

$$H(Traj) = (X *_d f)(Traj) = \sum_{i=0}^{n-1} f(i) \cdot x_{T-d \cdot i} \tag{6}$$

where n represents the filter size, d represents the dilation factor, and $T - d \cdot i$ reflects the consideration of past time steps.

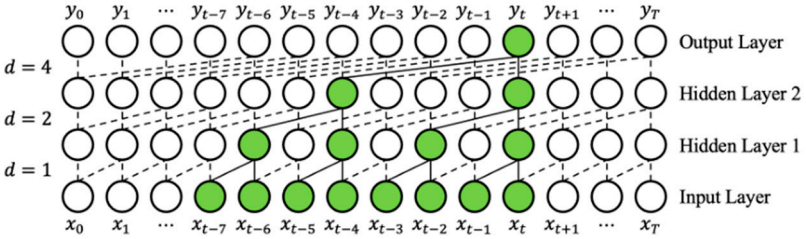


Figure 4. Dilated convolution structure.

By increasing the filter size n and adjusting the dilation factor d, TCN effectively expands the receptive field. This improvement enables the top layer output of the model to cover a wider range of input information. Additionally, the model enhances the overall computational efficiency by processing the same filters in parallel across layers. Figure 4 illustrates the dilated causal convolution stack structure with a filter size of $n = 2$ and a dilation factor of $d = [1, 2, 4]$. By introducing dilated convolution, the output y_t at time point t can aggregate input information from the time span x_{t-7} to x_t.

In addition to adjusting the filter size n and dilation factor d, the receptive field size of the TCN can also be further expanded by increasing the number of hidden layers. However,

an overly deep network structure may affect model training stability and cause gradient vanishing issues. To address this challenge, TCN introduces the residual block design. The specific details of the residual block are shown in Figure 5. This design not only helps mitigate the gradient vanishing problem, but it also improves the training efficiency and performance of the deep network.

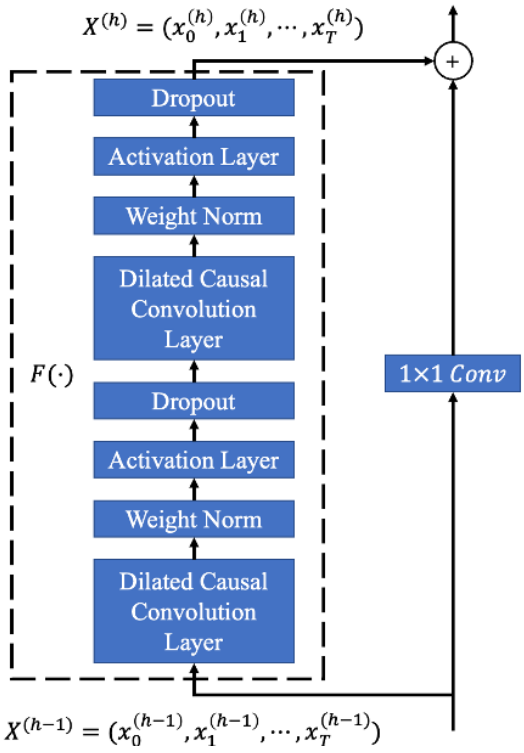


Figure 5. Residual block structure.

Inside the residual block, one branch is responsible for performing the transformation $F(\cdot)$ on the input $X_{(h-1)}$. Additionally, to maintain the number of feature maps during parallel processing, the residual block includes a branch that performs a simple 1×1 convolution transformation. Therefore, the output X_h of the h-th residual block can be expressed as

$$X_h = \delta[F(X_{h-1}) + X_{h-1}] \tag{7}$$

In this framework, $\delta(\cdot)$ denotes an activation operation. Notably, $F(\cdot)$ is a sequence of multiple transformation operations, including dilated causal convolution layers, weight normalization, activation layers, and dropout. More specifically, the dilated causal convolution layer combines the previously mentioned causal convolution and dilated convolution to extract hidden features from the input data. Weight normalization serves to accelerate the training process by controlling the range of weights, while the activation layer employs the well-converging rectified linear unit (ReLU). Additionally, dropout is used as a regularization technique to help address potential overfitting issues in the deep network.

Figure 6 illustrates a deep TCN formed by stacking h residual blocks. Building a deep TCN allows the network to look further back in time to extract features, meaning that each convolution in the output layer can receive more information from the convolutions in the input layer.

To extract long-term time series features suitable for load forecasting, Figure 7 presents a feature extraction network based on the TCN shown in Figure 6. This network captures deep and long-term dependencies in the time series data by comprehensively applying the TCN's dilated convolution, causal convolution, and residual blocks.

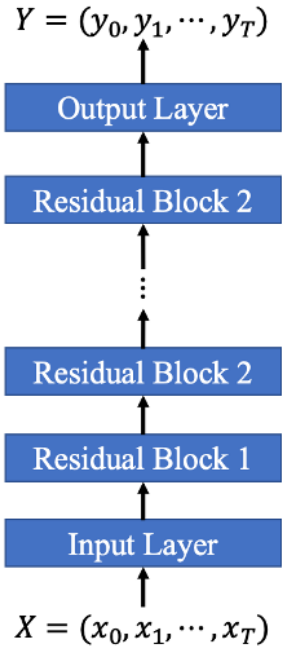


Figure 6. Deep TCN structure.

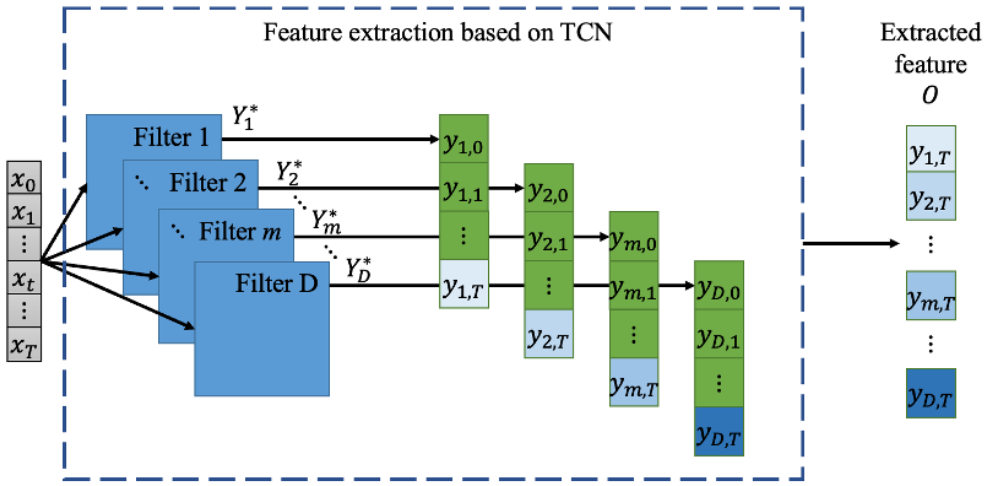


Figure 7. TCN-based feature extraction network structure.

The specific network process can be outlined as follows. Initially, the one-dimensional feature $X = (x_0, x_1, \cdots, x_t, \cdots, x_T)$ is input into D filters of the TCN to obtain Y^* with dimensions $D \times T$, i.e., $Y_1^*, Y_2^*, \cdots, Y_m^*, \cdots, Y_D^*$, where the m-th vector is represented as $Y_m^* = (y_{m,0}, y_{m,1}, \cdots, y_{m,T})$, and $m = 1, 2, \cdots, D$. Subsequently, the last element of each one-dimensional vector Y_m^* is concatenated and merged with the output y_t from the WT, and then input into the fully connected layer. Finally, the features extracted in the fully connected layer $O = (y_{1.T}, y_{2.T}, \cdots, y_{m.T}, \cdots, y_{D.T})$ are used as the GRU input for ship trajectory prediction.

2.3.3. Gated Recurrent Unit

In 2014, Cho et al. [23] introduced the GRU, providing a simplified alternative to the LSTM unit. As a more efficient variant of the LSTM mechanism, the GRU is characterized by fewer parameters and can achieve higher accuracy in certain cases. Figure 8 shows a representation of a GRU unit, where x_t is the input sequence, h_{t-1} is the hidden state vector at the previous time step, and h_t is the current state.

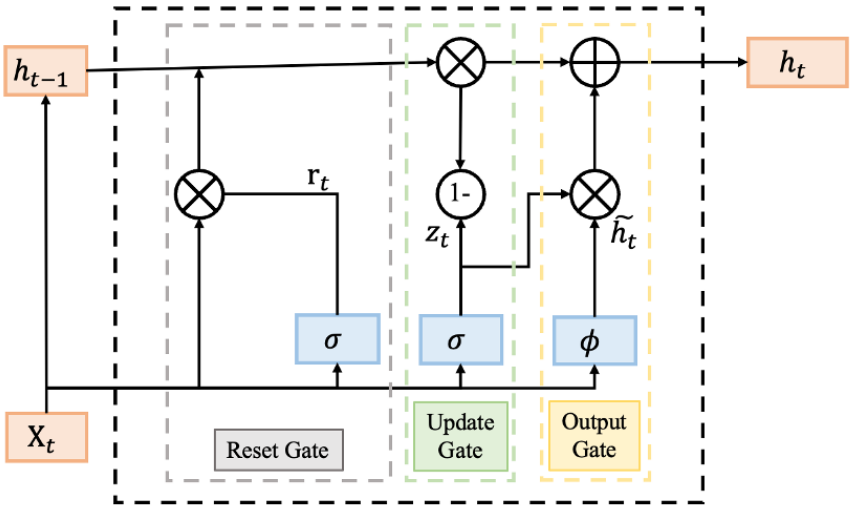


Figure 8. GRU structure.

2.3.4. Multi-Head Attention Mechanisms

To fully exploit the correlations of data at multiple levels, a multi-head attention mechanism was adopted, thereby enhancing the stability of feature learning in the model [29,30]. More specifically, the *K*-independently operating attention mechanisms focus on different levels of information, in addition to transforming features, and aggregating the outputs of the *K*-independent features to form a comprehensive output feature representation. This approach strengthens the ability of the model to capture multidimensional correlations in the data by combining multiple independent features.

$$Po_i^{l+1} = ||_{k=1}^{K} \sigma\left(\sum_{j \in N(i)} \alpha_{ij}^{K} W^{K} Po_j^{l}\right) \tag{8}$$

where $||$ represents the concatenation operation, a_{ij}^{K} is the normalized attention coefficient in the *k*th attention mechanism, and W^K is the corresponding weight matrix for the linear transformation in the *k*th attention mechanism. Through the parallel computation of each group, the grouped calculation of the attention coefficients for the different nodes improves the computational efficiency of the model, thereby enhancing the influences of the relevant nodes on the current node. This serves as a means of improving the feature extraction capability and robustness of the model.

2.3.5. Model Evaluation Indices

This study employed six evaluation metrics to quantify the trajectory prediction performance of the proposed hybrid model and common machine and deep learning methods from both global and local perspectives. In previous studies, the use of only one or two metrics to evaluate the performances of prediction methods has been criticized for introducing bias and distorting the results [1]. Therefore, it is recommended that a range of relevant factors and metrics be considered to obtain a comprehensive evaluation. The specific formulae for these six metrics are as follows

$$RMSE = \sqrt{\frac{1}{N}\sum_{i=1}^{N}\left(Po_i - \widehat{Po}_i\right)^2} \tag{9}$$

$$MAE = \frac{1}{N}\sum_{i=1}^{N}\left|Po_i - \widehat{Po}_i\right| \tag{10}$$

$$SMAPE = \frac{1}{N}\sum_{i}^{N}\frac{2\left|Po_i - \widehat{Po_i}\right|}{|Po_i| + \left|\widehat{Po_i}\right|} \tag{11}$$

$$FDE = \sqrt{\left[Po_n(lon) - \widehat{Po_n}(lon)\right]^2 + \left[Po_n(lat) - \widehat{Po_n}(lat)\right]^2} \tag{12}$$

$$FD = \max_{i\in[1,N]}\sqrt{\left[Po_i(lon) - \widehat{Po_i}(lon)\right]^2 + \left[Po_i(lat) - \widehat{Po_i}(lat)\right]^2} \tag{13}$$

$$AED = \frac{1}{N}\sum_{i=1}^{N}\sqrt{\left[Po_i(lon) - \widehat{Po_i}(lon)\right]^2 + \left[Po_i(lat) - \widehat{Po_i}(lat)\right]^2} \tag{14}$$

where N is the total number of test trajectory points, Po_i is the true value at the ith trajectory point, and $\widehat{Po_i}$ is the predicted value.

3. Results

To perform an experimental assessment of the developed model using an authentic AIS dataset, the suitability of WTG was evaluated in the coastal seas of Fujian. Figure 9a shows the location of the research area relative to China. The reliability of the WTG model was determined by examining two areas with different features, as shown in Figure 9b. The initial study location was the Minjiang River Estuary, as depicted in Figure 9c, which is somewhat open and heavily populated with large vessels. The second study location was the waters next to the Haitan Strait, as depicted in Figure 9d, which are characterized by several islets and small fishing boats.

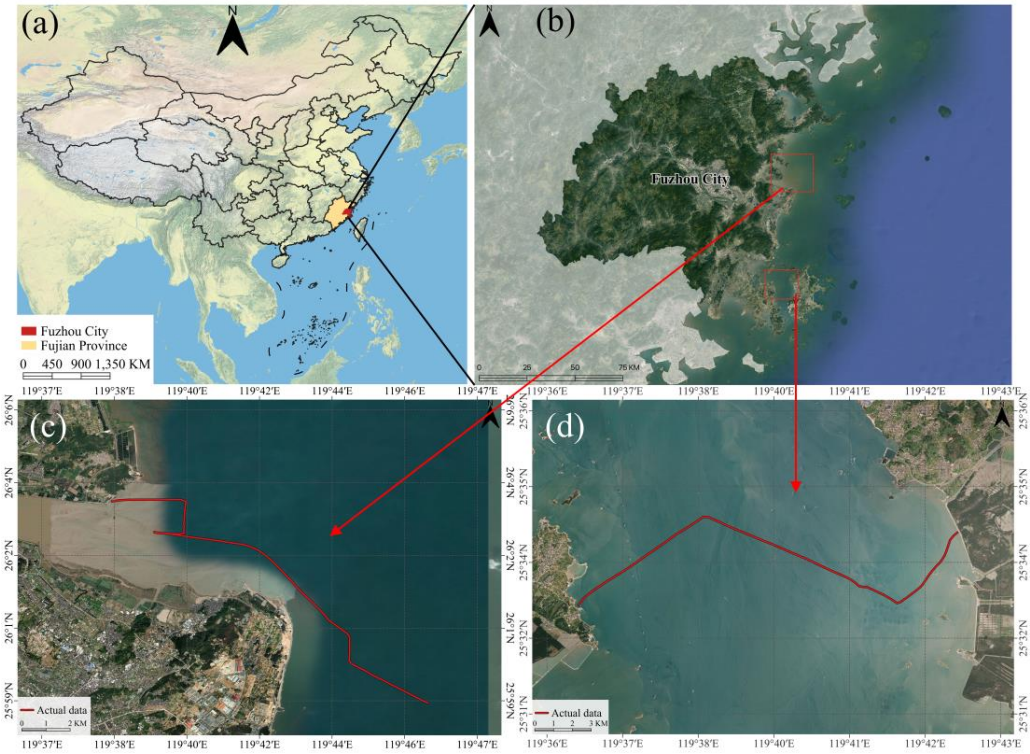


Figure 9. Location of the study area.

3.1. Experimental Settings

The efficacy of the proposed model was assessed by comparing it to four benchmark ship trajectory prediction models, namely the BP, CNN, RNN, LSTM and Transformer models. Ship trajectory prediction studies were performed using a macOS system featuring an M1 central processing unit (CPU). The model was developed using the PyTorch 2.4 module

in Python 3.10. The dataset was partitioned into three sections, namely the training, validation, and testing datasets. The Adaptive Moment Estimation (ADAM) technique was used during training to update the parameters dynamically by altering the learning rate according to the gradient of each parameter. The learning rate was set as 0.001. The model was configured with 120 nodes, wherein each node corresponds to a part of a divided trajectory. For the purpose of this study, the longitude and latitude coordinates of the ship's track recorded at 60 time points were used as the input data to forecast the coordinates at the 61st time point.

3.2. Prediction Results and Analysis

Five commonly used trajectory prediction measures (i.e., the average Euclidean distance, AED; the Fréchet distance, FD; the final displacement error, FDE; the mean absolute error, MAE; and the root mean squared error, RMSE) were employed to demonstrate the predictive performances of the different models for analysis. Lower values indicate superior forecasting performances. Thus, an efficacy assessment of the proposed model and the four standard models was performed on 164 trajectories in the test set. Table 2 displays the mean performances of the five prediction techniques across 20, 40, and 60 min prediction intervals, with the assessment outcomes of the WTG model being emphasized in bold. The proposed model demonstrated a superior performance compared to the four conventional trajectory prediction approaches across the five assessment metrics. These results therefore validated the capacity of the WTG model to capture the multimodal features of ship trajectories, identify significant long-term relationships, and precisely forecast ship routes.

Table 2. Prediction error of different models.

Metric	Time Length /min	Models					
		BP	**Transformer**	**CNN**	**RNN**	**LSTM**	**WTG**
AED	20	0.049	0.206	0.012	0.024	0.017	0.009
	40	0.049	0.208	0.011	0.025	0.015	0.009
	60	0.049	0.263	0.011	0.027	0.015	0.009
FD	20	0.086	0.121	0.019	0.038	0.024	0.016
	40	0.097	0.142	0.022	0.048	0.026	0.018
	60	0.109	0.168	0.026	0.055	0.028	0.021
FDE	20	0.049	0.120	0.010	0.025	0.015	0.010
	40	0.048	0.132	0.011	0.028	0.012	0.009
	60	0.059	0.134	0.011	0.032	0.015	0.010
MAE	20	0.012	0.050	0.005	0.008	0.005	0.005
	40	0.014	0.055	0.007	0.009	0.007	0.007
	60	0.015	0.063	0.008	0.010	0.008	0.008
RMSE	20	0.090	0.183	0.052	0.077	0.054	0.050
	40	0.105	0.185	0.069	0.089	0.069	0.067
	60	0.115	0.187	0.077	0.095	0.077	0.075

Subsequently, the evaluation results were visualized to more effectively compare the proposed model with the benchmark models. As shown in Table 2, the Transformer method performed the worst, likely due to the irregularity of the collected trajectory data and the large number of parameters, which led to model convergence failure. As a result, its error was more than twice that of the BP method. Additionally, the deep learning methods generally provided better predictive outcomes than machine learning methods. It was also observed that the prediction accuracy of the RNN model was significantly lower than that of the CNN and LSTM models. In the 60 min prediction test interval, the WTG model outperformed the best standard model, CNN, by 0.5% in the FD evaluation metric, 0.2% in both the AED and RMSE metrics, and 0.1% in the FDE metric.

3.2.1. Analysis of Results in the Minjiang Estuary

This example involves predicting the sailing trajectory that starts from the Minjiang Estuary and moves towards Taiwan. The prediction results displayed in Figure 10 indicate that the BP model exhibits the poorest predictive performance for Ship 1's trajectory. More specifically, at several points along the trajectory, the forecasted values exhibit a pattern comparable to the real values, but with notable discrepancies. This is likely due to the tendency of this strategy to frequently produce local optimal solutions in trials. In addition, the results show that the CNN, RNN, and LSTM models exhibited comparable predictive performances, particularly regarding their patterns. These three models may share the commonality of utilizing deep learning techniques to efficiently extract data attributes. The projected values of the CNN model were more accurate than those of the RNN model, perhaps because of its superior ability to extract hierarchical characteristics from trajectory data. Furthermore, the WTG model accurately predicted the trajectory and demonstrated the highest prediction accuracy among the models. Indeed, the WTG model efficiently incorporated the characteristics of time-series data at various frequencies. Figure 11 illustrates the discrepancy in the distance between the projected and actual locations of the various models. It can be seen that the BP model exhibited the lowest prediction stability compared to the other models. Although the projected values closely matched the actual values at certain points along the route, in general, there were notable discrepancies, with the greatest error surpassing 1.2 km. It can also be seen that the RNN, LSTM, and CNN models are relatively stable, but that they still exhibit large prediction errors, ranging from 400 to 800 m for RNN and LSTM, and exceeding 100 m for CNN. In contrast, the WTG model demonstrated a superior prediction stability compared to other benchmark models, with errors typically <100 m.

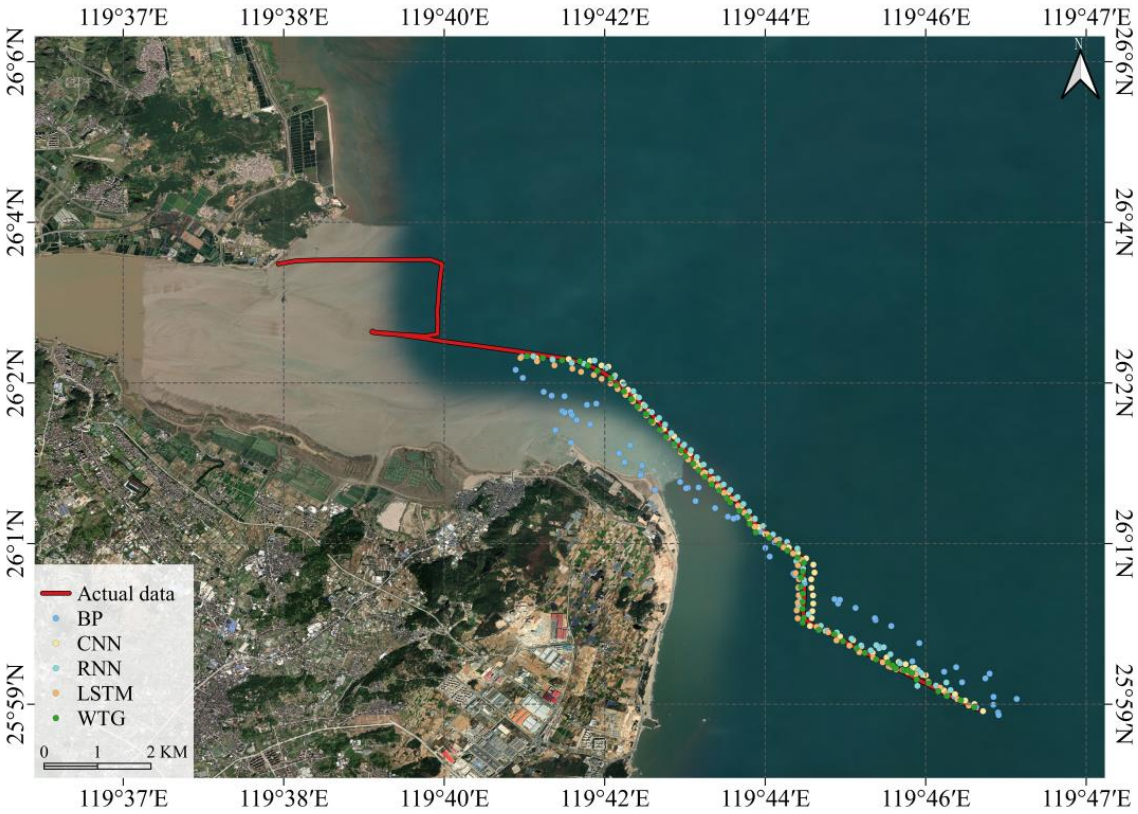


Figure 10. Results of experiments comparing multiple models for predicting the trajectory of Ship 1.

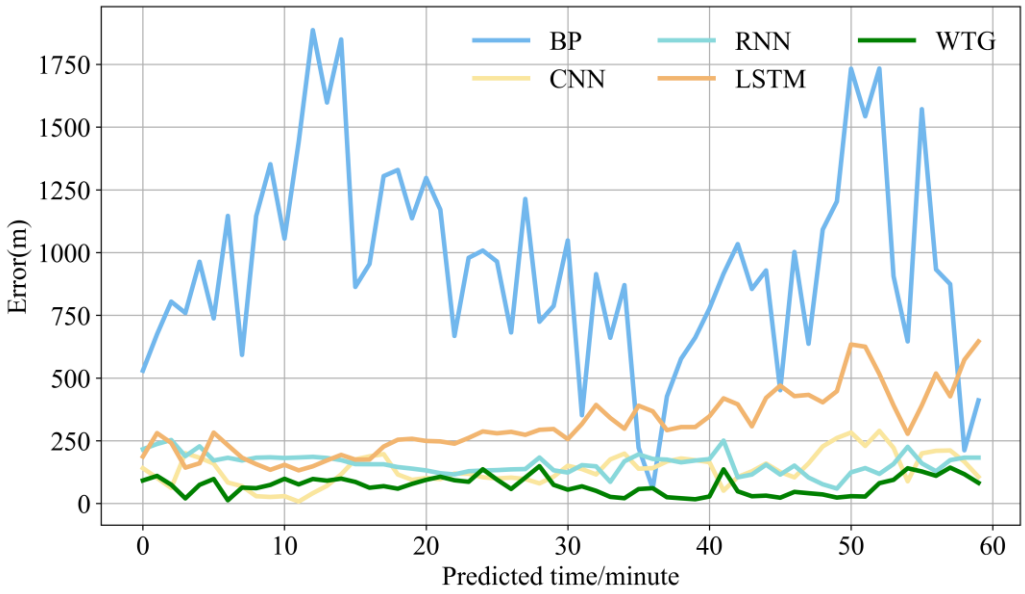


Figure 11. Distance error with time iteration for Ship 1.

Figures 12 and 13 show the six evaluation metrics of Case A, comparing the baseline models BP, CNN, and RNN, while also comparing the CNN model with the proposed WTG model. Figure 12 shows the calculation results for the predicted values before denormalization. It can be seen that the BP neural network exhibits the worst prediction performance (i.e., the largest error rate) in the three evaluation metrics for this test trajectory, followed by the RNN method. The CNN and LSTM methods demonstrated superior prediction performances for these three metrics, while the WTG achieved the lowest values for each evaluation metric. Figure 13 displays the actual distance error calculations after post-denormalization, wherein the BP neural network demonstrated the highest predicted distance error and the greatest error, reaching 1846 m. The FDE and ADE values for the CNN, LSTM, and WTG models were all within 200 m, with the WTG model showing the best performance for each evaluation metric.

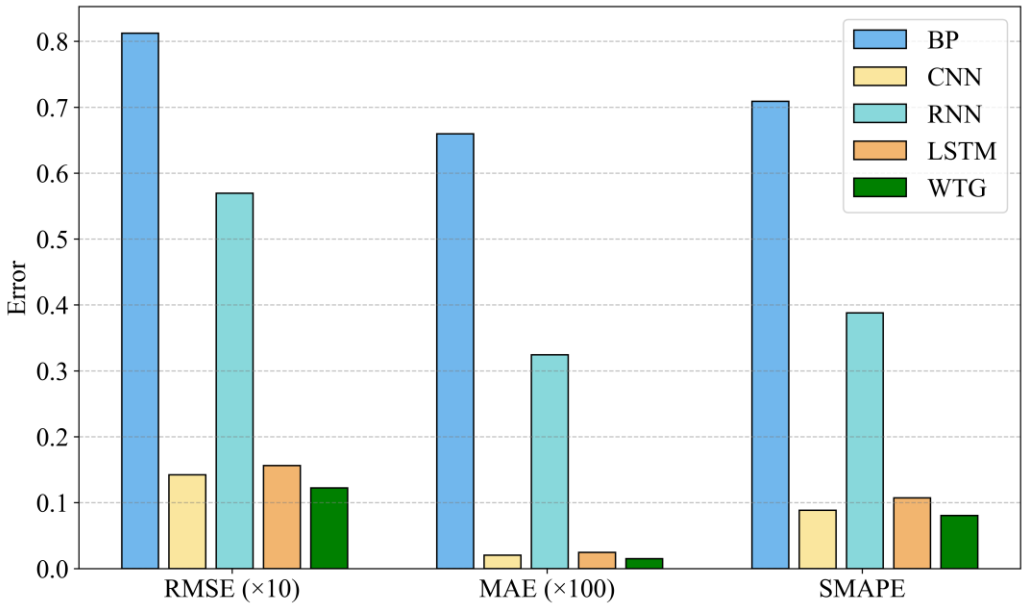


Figure 12. Visualization of the RMSE, MAE, and SMAPE metrics results for the Minjiang Estuary.

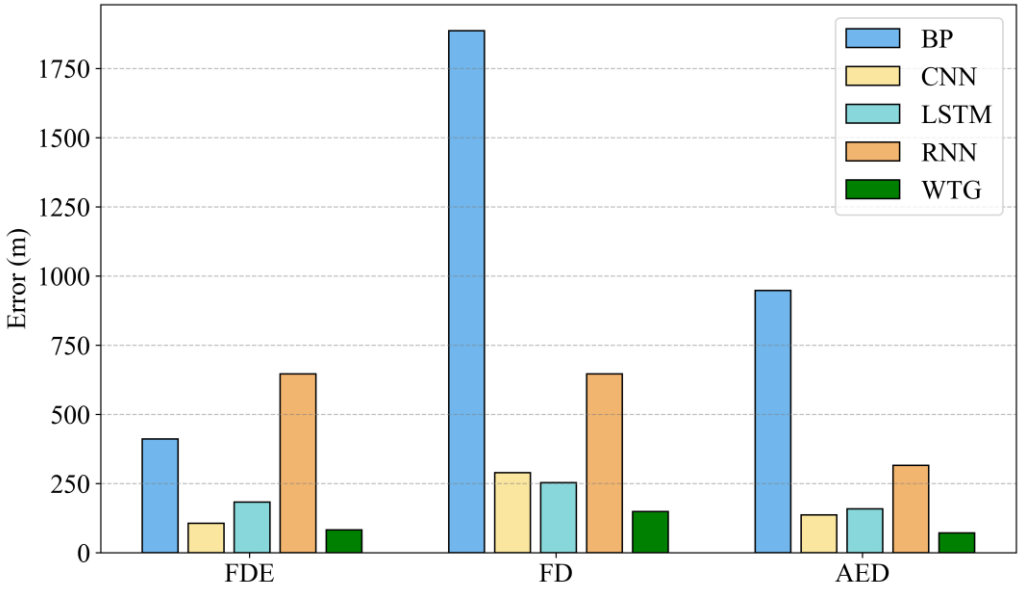


Figure 13. Visualization of the FDE, FD, and AED metrics results for the Minjiang Estuary.

In another example of a ship trajectory starting from the Minjiang Estuary, the prediction results shown in Figure 14 indicated that the BP model performed the worst in predicting Ship 1's trajectory, as its predicted movement trend was entirely inconsistent with the actual trajectory. As illustrated in Figure 15, the RNN and LSTM models produced relatively better results, with prediction errors of around 600 m. The CNN model outperformed both LSTM and RNN, with error margins of within 400 m. In contrast, during the first 45 min, the WTG model exhibited smaller prediction errors than the CNN model and demonstrated superior stability, with overall prediction errors remaining below 200 m.

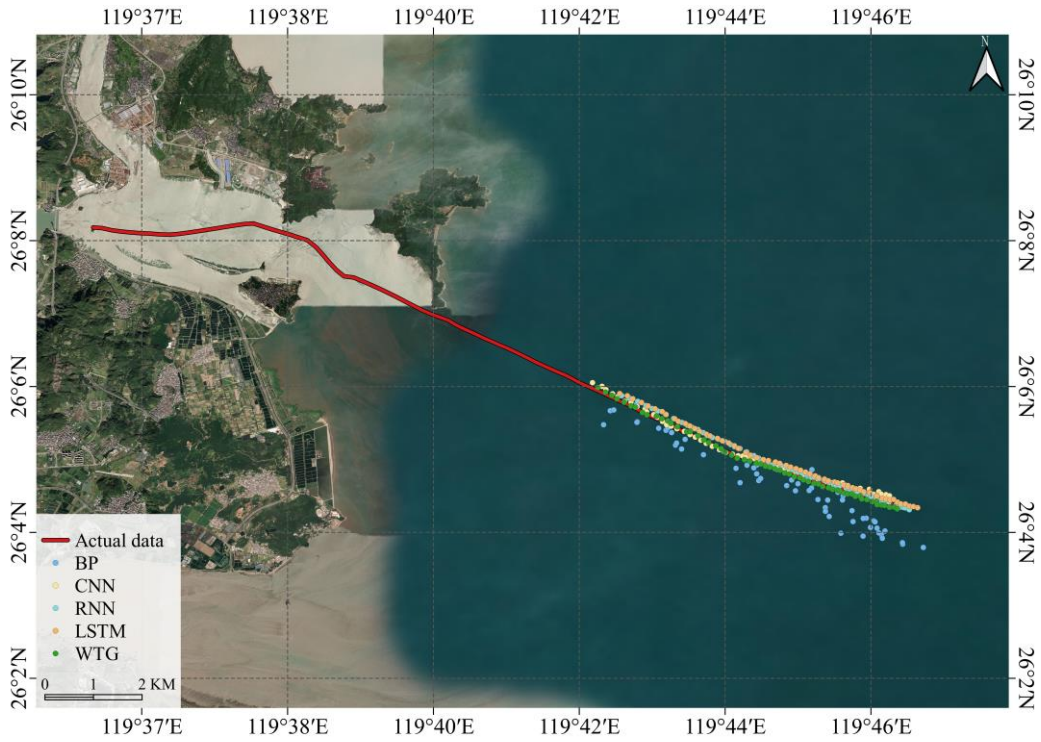


Figure 14. Results of experiments comparing multiple models for predicting the trajectory of Ship 2.

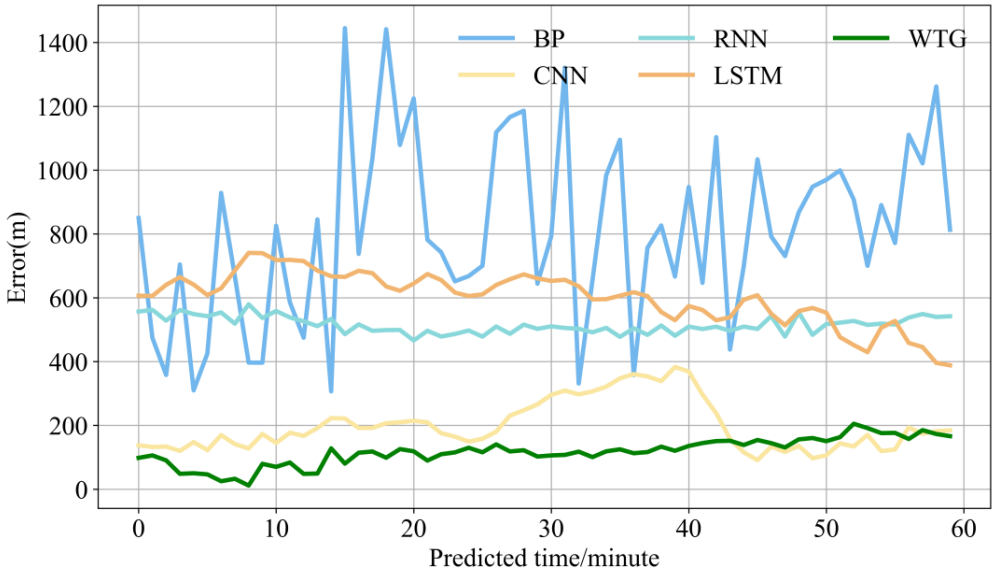


Figure 15. Distance error with time iteration for Ship 2.

Figure 16 presents the FD, FD, and AED evaluation metrics for Case B, comparing the baseline models BP, CNN, and RNN, as well as the CNN model with the proposed WTG model. The WTG model performed the best across all evaluation metrics, with each metric value being less than 200 m. However, the prediction error for the LSTM model was significantly higher in Case B compared to Case A.

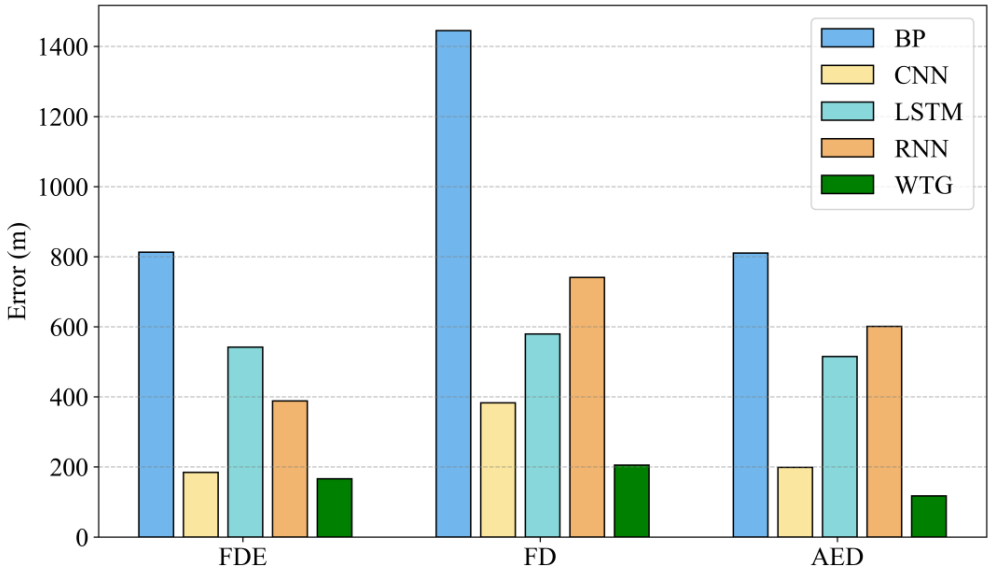


Figure 16. Visualization of the FDE, FD, and AED metrics results for Ship 2.

3.2.2. Analysis of Results in the Haitan Strait

This example involves predicting a journey trajectory that starts at the northwest corner of Pingtan Island and travels through the Haitan Strait. The canal of the strait is clogged with numerous islands, and there are multiple turning places along the trajectory. This trajectory was selected for testing to demonstrate the effectiveness of the proposed prediction approach for intricate trajectories. Figure 17 presents the forecast results, wherein it can be seen that the BP model showed the poorest accuracy in predicting Ship 3's trajectory, with notable variations from the actual path. From Figure 17, it is evident that there are notable discrepancies between the anticipated and actual trajectory trends. The gradual alignment of the projected and actual trajectories after 30 min may be a result of coincidental trajectory intersections, rather

than indicating a reduction in the prediction error. The RNN model exhibited the poorest predictive performance when compared to the other deep learning models, and variations existed in the exact course. Furthermore, compared to the other deep learning models, the RNN model displayed notable discrepancies in its forecasted values prior to the inflection points in the trajectory. Moreover, it was found that the predicted values for the CNN model were more accurate for the actual trajectory than those of the RNN and LSTM models. The CNN prediction errors, as illustrated in Figure 18, were limited to a range of 200 m, likely due to the superior ability of the CNN model to extract hierarchical characteristics from the trajectory data. Notably, the predicted trajectory for the WTG model was observed to closely align with the actual trajectory, demonstrating the highest prediction accuracy among the examined models. Additionally, the WTG model efficiently incorporated the characteristics of time-series data at various frequencies.

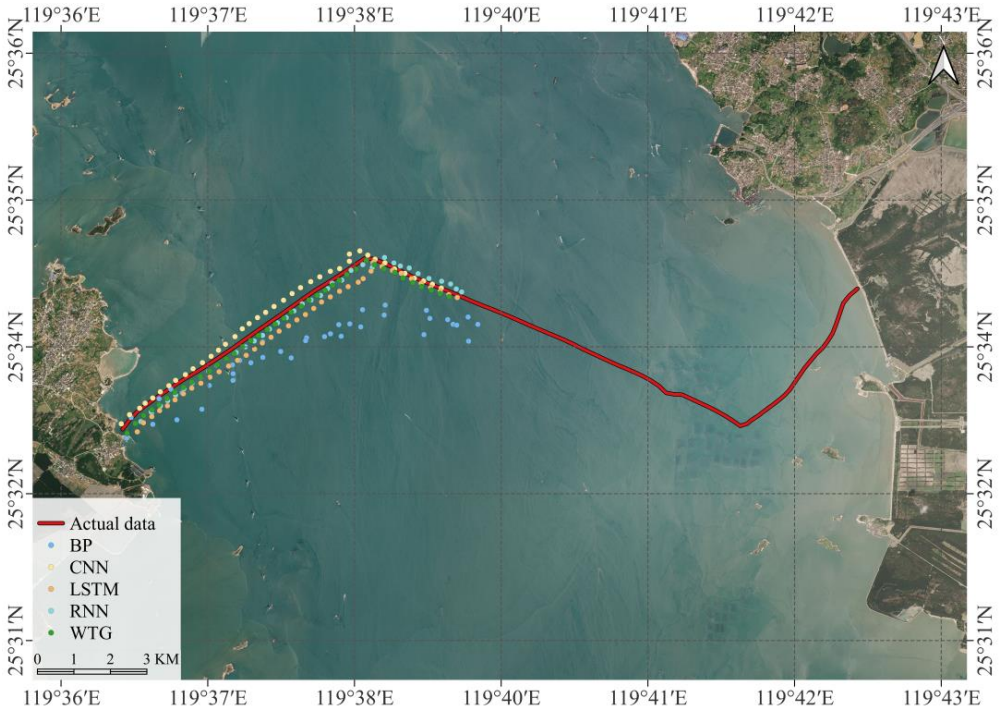


Figure 17. Results of experiments comparing multiple models for predicting the trajectory of Ship 3.

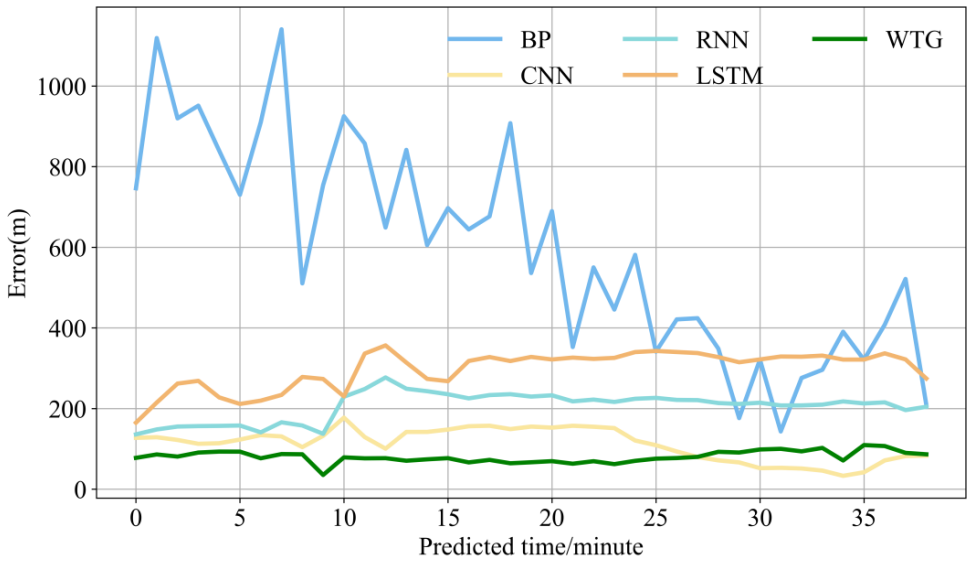


Figure 18. Distance error with time iteration for Ship 3.

In complex waterways, navigation trajectories have many turning points, and the prediction accuracies of the SOG and COG also affect future trajectory predictions. As shown in Figure 19, the BP and RNN models exhibited relatively large errors in predicting the SOG, whereas the CNN, LSTM, and WTG models demonstrated similar SOG prediction errors. From the comparison in Table 3, it can be seen that the WTG model shows the smallest average prediction error. Moreover, Figure 20 indicates that the RNN model exhibits the poorest performance in predicting the COG, whereas the CNN and WTG models gave similar prediction values.

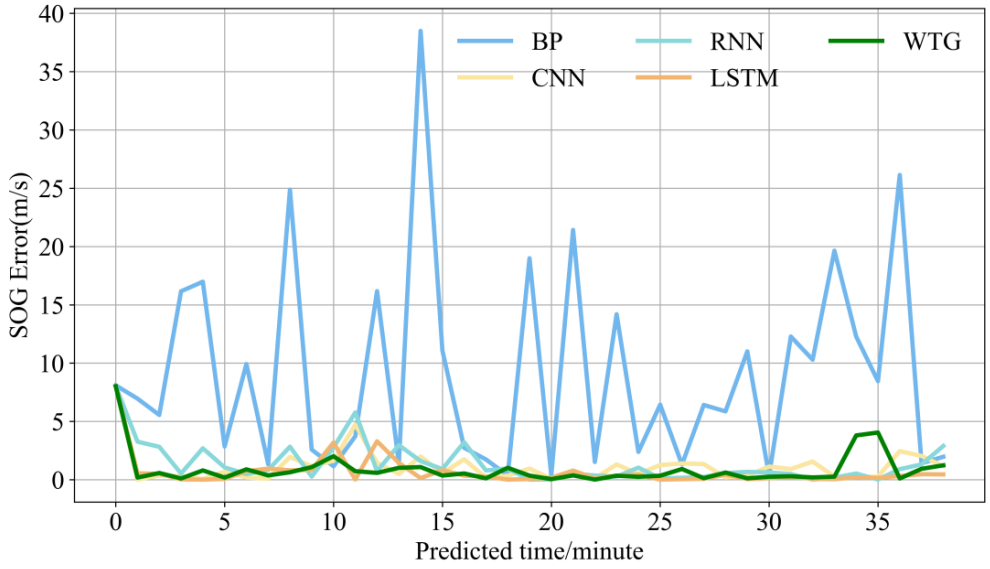


Figure 19. Absolute errors for the SOG predictions by the different models.

Table 3. Average errors for the SOG and COG predictions by the different models.

	BP	CNN	RNN	LSTM	WTG
SOG	0.0393	0.0062	0.0235	0.0074	0.0050
COG	0.0414	0.0123	0.1196	0.0220	0.01330

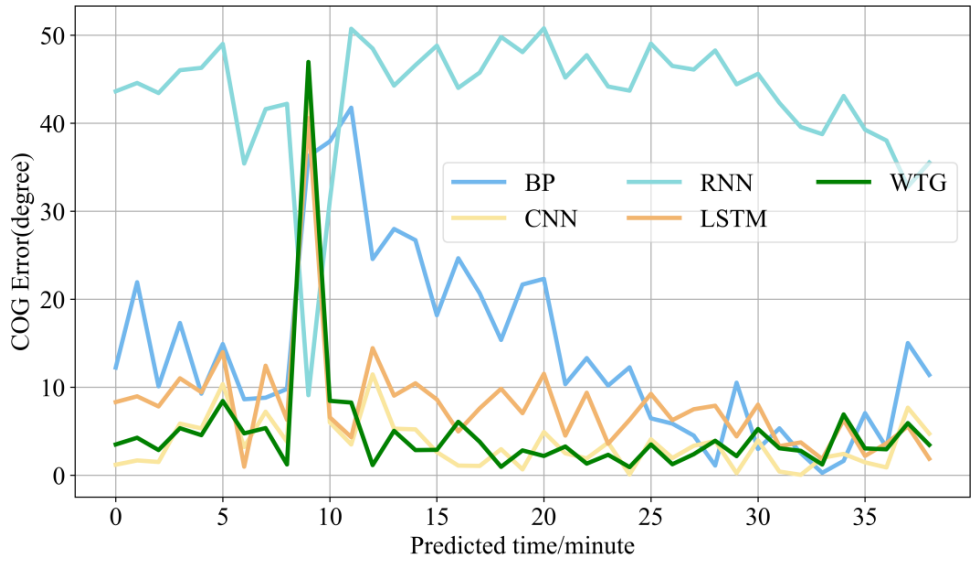


Figure 20. Absolute errors for the COG predictions by the different models.

To further demonstrate the prediction performances of the different models, the AED, FD, FDE, MAE, RMSE, and SMAPE metrics were employed. Figures 21 and 22 show the

six evaluation metrics of Case A, comparing the baseline models BP, CNN, and RNN, while also comparing the CNN model with the proposed WTG model. Figure 21 shows that the BP neural network and RNN models exhibited poor prediction performances in the three evaluation metrics for this test trajectory. In the RMSE and MAE metrics, the BP neural network outperformed the RNN model, possibly because the BP neural network was able to provide more accurate predictions of the overall ship direction, despite being unable to capture finer-scale features in the trajectory data. The CNN and LSTM models exhibited superior prediction performances in these three metrics, with the CNN model outperforming the LSTM model. Moreover, the WTG model achieved the lowest values for each evaluation metric. Figure 22 shows the actual distance error calculations after denormalization, wherein it can be seen that the BP neural network exhibited the largest predicted distance error, although it was smaller than that obtained in the open waters of the Minjiang Estuary, with a maximum value of 1208 m. For the CNN and WTG models, all three of the error values were within 200 m; however, the WTG model exhibited a superior performance to the CNN model and was the most accurate among the six models.

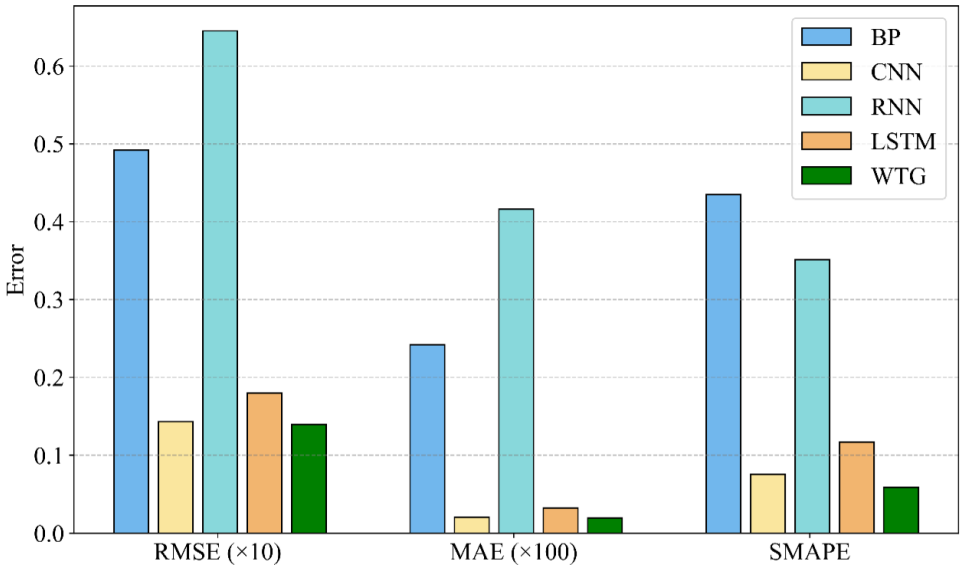


Figure 21. Visualization of the RMSE, MAE, and SMAPE metric results for the Haitan Strait.

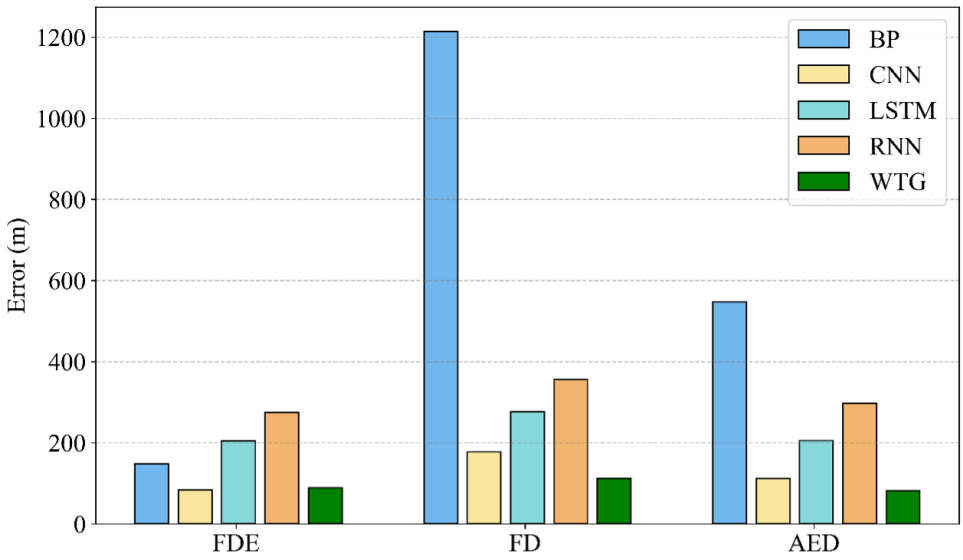


Figure 22. Visualization of the FDE, FD, and AED metric results for the Haitan Strait.

3.2.3. Prediction Performance at Different Time Intervals

To evaluate ship trajectory prediction performance under data loss scenarios caused by adverse sea conditions, AIS data were downsampled to simulate varying levels of data availability. Figure 23 presents the RMSE of trajectory predictions over the next 20 min for AIS data at different time intervals. It can be observed that the BP model shows the most unstable performance, with prediction errors increasing as the time interval widens. In contrast, deep learning models, including the WTG model, demonstrate relatively stable prediction performance for AIS data sampled at intervals of up to 10 min. This suggests that the model developed in this study is robust even in extreme scenarios involving data sparsity.

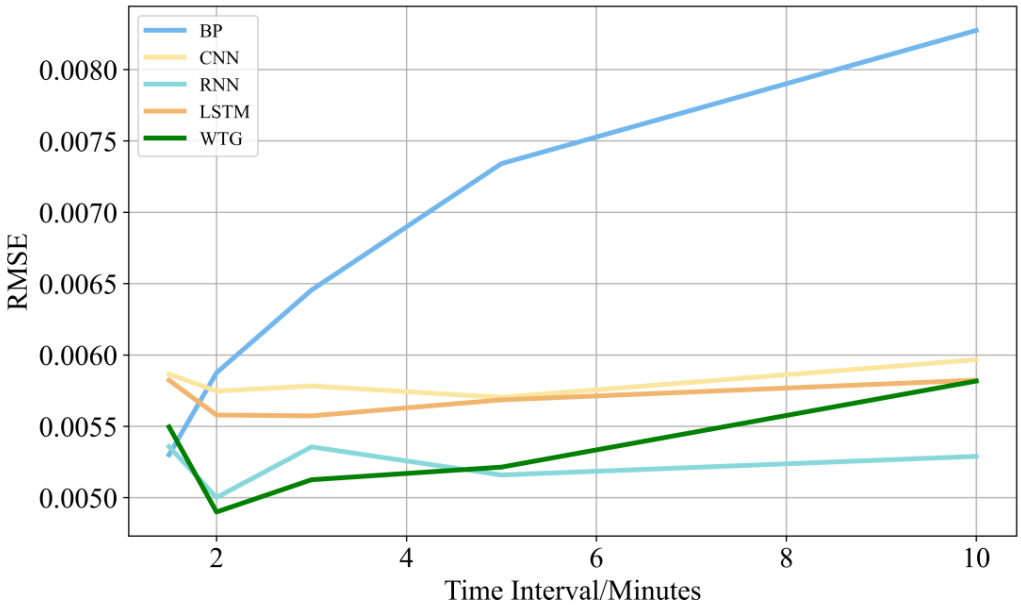


Figure 23. Visualization of trajectory prediction RMSE at different time intervals.

3.2.4. Ablation Studies

Ablation experiments were conducted using the WTG model to determine the significance of each component of the proposed model. The learning rate was set to 0.001 to train the GRU and TCN modules. The model was evaluated using 164 trajectories from the test set, and the performance outcomes are listed in Table 4. As indicated, the performances of the individual components were inferior to that of the WTG model, and it was found that combination of the TCN module with the GRU model led to an enhanced prediction accuracy.

Table 4. Impact of the TCN and GRU components on the prediction results.

	TCN	GRU	WTG
AED	0.351	0.204	0.009
FD	0.430	0.357	0.016
FDE	0.391	0.172	0.009
MAE	0.075	0.032	0.005
RMSE	0.267	0.159	0.051
SMAPE	2.147	1.414	0.487

4. Conclusions

This study proposed an innovative WTG model for forecasting ship paths using automatic identification system (AIS) data. Specifically, the model employs wavelet transform for feature extraction and integrates TCN with GRU architectures, utilizing an improved sparse and high-dimensional representation of AIS data to analyze complex patterns in ship

movements. Experiments conducted with real AIS data demonstrated that the proposed WTG model significantly enhances the accuracy of ship trajectory prediction. This advancement aids maritime traffic management authorities in optimizing route planning, reducing channel congestion, and thereby improving overall transportation efficiency. Additionally, it facilitates the timely identification of abnormal ship behaviors, preventing maritime accidents and ensuring navigational safety. Furthermore, the model assists ship management companies and logistics enterprises in dynamic scheduling and resource allocation, thereby lowering operational costs and enhancing service quality.

However, this study has certain limitations. Firstly, the performance of the WTG model under extreme sea conditions or in complex marine environments has not been fully evaluated. Future research should incorporate more environmental variables, such as sea state data, to enhance the model's robustness. Secondly, due to the limitations of AIS data, the model's performance under different types of vessels and various weather conditions has not been tested. Therefore, future research should focus on further optimizing the model and expanding its application scope to improve its predictive capabilities in different maritime regions and sea conditions, thus overcoming the current limitations.

Author Contributions: Q.G. and D.D. conceived of the original idea of this study, and designed, organized, and supervised the entire investigation; X.L. collected, processed and analyzed the data, and wrote the article; Y.D. assisted in data preprocessing and analysis; C.L. assisted in data collection; Z.W. assisted in manuscript preparation and revision. All authors have read and agreed to the published version of the manuscript.

Funding: This research is supported by the special fund for Fujian Province to promote the high-quality development of the marine and fishery industry (FJHYF-ZH-2023-01).

Data Availability Statement: The dataset related to this article can be found at The China Ports Network (https://www.chinaports.com, accessed on 26 March 2024).

Conflicts of Interest: The authors declare no conflicts of interest.

Abbreviations

The following abbreviations are used in this manuscript:

Adam	Adaptive moment estimation
AED	Average Euclidean distance
AIS	Automatic identification system
Bi-LSTM	Bidirectional long short-term memory
BP	Back propagation
COG	Course over ground
DWT	Discrete wavelet transform
FD	Fréchet distance
FDE	Final displacement error
GRU	Gated recurrent units
LSTM	Long short-term memory
MAE	Mean absolute error
PSO-LSTM	Particle swarm optimization long short-term memory
RMSE	Root mean squared error
ReLU	Rectified linear unit
SMAPE	Symmetric mean absolute percentage error
SOG	Speed over ground
STFT	Short-time Fourier transform
TCN	Temporal convolutional networks
WT	Wavelet transform

References

1. Yang, D.; Wu, L.; Wang, S.; Jia, H.; Li, K.X. How big data enriches maritime research—A critical review of Automatic Identification System (AIS) data applications. *Transp. Rev.* **2019**, *39*, 755–773. [CrossRef]
2. Bao, K.; Bi, J.; Gao, M.; Sun, Y.; Zhang, X.; Zhang, W. An improved ship trajectory prediction based on AIS data using MHA-BiGRU. *J. Mar. Sci. Eng.* **2022**, *10*, 804. [CrossRef]
3. Xiao, Y.; Li, X.; Yao, W.; Chen, J.; Hu, Y. Bidirectional data-driven trajectory prediction for intelligent maritime traffic. *IEEE Trans. Intell. Transp. Syst.* **2022**, *24*, 1773–1785. [CrossRef]
4. Li, X.; Ying, X.; Chuah, M.C. Grip: Graph-based interaction-aware trajectory prediction. In Proceedings of the 2019 IEEE Intelligent Transportation Systems Conference (ITSC), Auckland, New Zealand, 27–30 October 2019; pp. 3960–3966.
5. Korbmacher, R.; Tordeux, A. Review of pedestrian trajectory prediction methods: Comparing deep learning and knowledge-based approaches. *IEEE Trans. Intell. Transp. Syst.* **2022**, *23*, 24126–24144. [CrossRef]
6. Atkeson, C.; McIntyre, J. Robot trajectory learning through practice. In Proceedings of the 1986 IEEE International Conference on Robotics and Automation, San Francisco, CA, USA, 7–10 April 1986; pp. 1737–1742.
7. Li, H.; Liu, J.; Yang, Z.; Liu, R.W.; Wu, K.; Wan, Y. Adaptively constrained dynamic time warping for time series classification and clustering. *Inf. Sci.* **2020**, *534*, 97–116. [CrossRef]
8. Tu, E.; Zhang, G.; Rachmawati, L.; Rajabally, E.; Huang, G.-B. Exploiting AIS data for intelligent maritime navigation: A comprehensive survey from data to methodology. *IEEE Trans. Intell. Transp. Syst.* **2017**, *19*, 1559–1582. [CrossRef]
9. Zhang, X.; Fu, X.; Xiao, Z.; Xu, H.; Qin, Z. Vessel trajectory prediction in maritime transportation: Current approaches and beyond. *IEEE Trans. Intell. Transp. Syst.* **2022**, *23*, 19980–19998. [CrossRef]
10. Jiang, B.; Zhou, W.; Chen, X. Ship trajectory prediction algorithm based on polynomial Kalman filter. *Signal Process.* **2019**, *35*, 741–746.
11. Guo, S.; Liu, C.; Guo, Z.; Feng, Y.; Hong, F.; Huang, H. Trajectory prediction for ocean vessels base on K-order multivariate Markov chain. In Proceedings of the Wireless Algorithms, Systems, and Applications: 13th International Conference, WASA 2018, Tianjin, China, 20–22 June 2018; pp. 140–150.
12. Zhou, H.; Chen, Y.; Zhang, S. Ship trajectory prediction based on BP neural network. *J. Artif. Intell.* **2019**, *1*, 29. [CrossRef]
13. Hu, Y.; Xia, W.; Hu, X.; Sun, H.; Wang, Y. Vessel trajectory prediction based on recurrent neural network. *Syst. Eng. Electron.* **2020**, *42*, 871–877.
14. Quan, B.; Yang, B.; Hu, K.; Guo, C.; Li, Q. Ship trajectory prediction model based on LSTM. *Comput. Sci.* **2018**, *45*, 126–131.
15. Zhao, C.; Zhuang, J.; Cheng, X.; Li, Y.; Guo, D. Ship trajectory prediction of RNN-Bi-LSTM based on characteristic attention mechanism. *J. Guangdong Ocean. Univ.* **2022**, *42*, 102–109.
16. Jahangard, S.; Hayat, M.; Rezatofighi, H. Real-time trajectory-based social group detection. In Proceedings of the 2023 IEEE/RSJ International Conference on Intelligent Robots and Systems (IROS), Detroit, MI, USA, 1–5 October 2023; pp. 1901–1908.
17. Bai, S.; Kolter, J.Z.; Koltun, V. An empirical evaluation of generic convolutional and recurrent networks for sequence modeling. *arXiv* **2018**, arXiv:1803.01271.
18. Hewage, P.; Behera, A.; Trovati, M.; Pereira, E.; Ghahremani, M.; Palmieri, F.; Liu, Y. Temporal convolutional neural (TCN) network for an effective weather forecasting using time-series data from the local weather station. *Soft Comput.* **2020**, *24*, 16453–16482. [CrossRef]
19. Ang, J.-S.; Ng, K.-W.; Chua, F.-F. Modeling time series data with deep learning: A review, analysis, evaluation and future trend. In Proceedings of the 2020 8th International Conference on Information Technology and Multimedia (ICIMU), Selangor, Malaysia, 24–26 August 2020; pp. 32–37.
20. Zhao, L.; Shi, G.; Yang, J. Ship trajectories pre-processing based on AIS data. *J. Navig.* **2018**, *71*, 1210–1230. [CrossRef]
21. Zhao, J.; Yan, Z.; Chen, X.; Han, B.; Wu, S.; Ke, R. k-GCN-LSTM: A k-hop Graph Convolutional Network and Long–Short-Term Memory for ship speed prediction. *Phys. A Stat. Mech. Its Appl.* **2022**, *606*, 128107. [CrossRef]
22. Zhang, D.; Li, J.; Wu, Q.; Liu, X.; Chu, X.; He, W. Enhance the AIS data availability by screening and interpolation. In Proceedings of the 2017 4th International Conference on Transportation Information and Safety (ICTIS), Banff, AB, Canada, 8–10 August 2017; pp. 981–986.
23. Haibing, H.; Zheng, X.; Yin, J.; Wang, Y. Research on O-ring dimension measurement algorithm based on cubic spline interpolation. *Appl. Sci.* **2021**, *11*, 3716. [CrossRef]
24. Cho, K. Learning phrase representations using RNN encoder-decoder for statistical machine translation. *arXiv* **2014**, arXiv:1406.1078.
25. Zhang, X.; Liu, G.; Hu, C.; Ma, X. Wavelet analysis based hidden Markov model for large ship trajectory prediction. In Proceedings of the 2019 Chinese Control Conference (CCC), IEEE, Guangzhou, China, 27–30 July 2019; pp. 2913–2918.
26. Zhu, W.; Li, X.; Liu, C.; Xue, F.; Han, Y. An STFT-LSTM system for P-wave identification. *IEEE Geosci. Remote Sens. Lett.* **2019**, *17*, 519–523. [CrossRef]
27. Abedinia, O.; Lotfi, M.; Bagheri, M.; Sobhani, B.; Shafie-Khah, M.; Catalão, J.P. Improved EMD-based complex prediction model for wind power forecasting. *IEEE Trans. Sustain. Energy* **2020**, *11*, 2790–2802. [CrossRef]
28. Gárate-Escamila, A.K.; El Hassani, A.H.; Andrès, E. Classification models for heart disease prediction using feature selection and PCA. *Inform. Med. Unlocked* **2020**, *19*, 100330. [CrossRef]

29. Vaswani, A.; Shazeer, N.; Parmar, N.; Uszkoreit, J.; Jones, L.; Gomez, A.N.; Kaiser, Ł.; Polosukhin, I.J. Attention is all you need. In Proceedings of the 31st Conference on Neural Information Processing Systems (NIPS 2017), Long Beach, CA, USA, 4–9 December 2017; Volume 30.
30. Busbridge, D.; Sherburn, D.; Cavallo, P.; Hammerla, N.Y. Relational graph attention networks. *arXiv* **2019**, arXiv:1904.05811.

Disclaimer/Publisher's Note: The statements, opinions and data contained in all publications are solely those of the individual author(s) and contributor(s) and not of MDPI and/or the editor(s). MDPI and/or the editor(s) disclaim responsibility for any injury to people or property resulting from any ideas, methods, instructions or products referred to in the content.